Applications of Gravitational Lensing In X-ray Astronomy

George Chartas, Penn State University

3rd INTERNATIONAL X-RAY ASTRONOMY SCHOOL

OVERVIEW

- Gravitational Lensing; Basics
- Applications of Gravitational Lensing in X-ray Astronomy
  - Observing distant and faint objects via the Magnification Effect
  - Imaging of AGN Accretion Disks via Microlensing
  - Constraining Cosmological Parameters
- Future Prospects

Gravitational Lensing; Basics

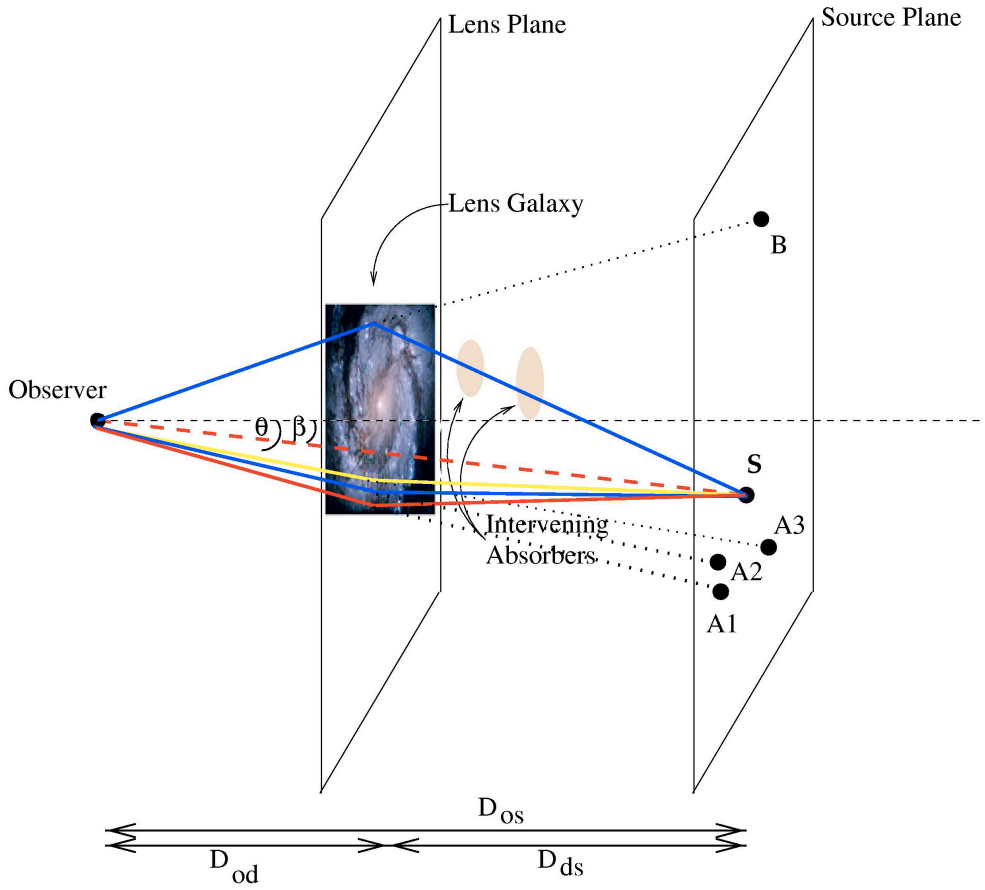

Conceptual diagram of the gravitational deflection of light in a quad GL system.

Gravitational Lensing; Basics

The two-dimensional **lens equation** is: $\vec{\eta} = \vec{\xi} - D_{ds}\vec{\hat{\alpha}}(\vec{\xi})$

The reduced deflection angle is : $\vec{\hat{\alpha}} = \frac{D_{ds}}{D_{os}}\vec{\alpha}$

The position vector in the lens plane is : $\vec{\xi} = D_{ds}\vec{\theta}$

The deflection angle at position $\vec{\xi}$ is the sum of the deflections due to all the mass elements in the lens plane :

$$\vec{\hat{\alpha}}(\vec{\xi}) = \frac{4G}{c^2}\int \frac{(\vec{\xi} - \vec{\xi}')\Sigma(\vec{\xi}')}{|\vec{\xi} - \vec{\xi}'|^2} d^2\xi'$$

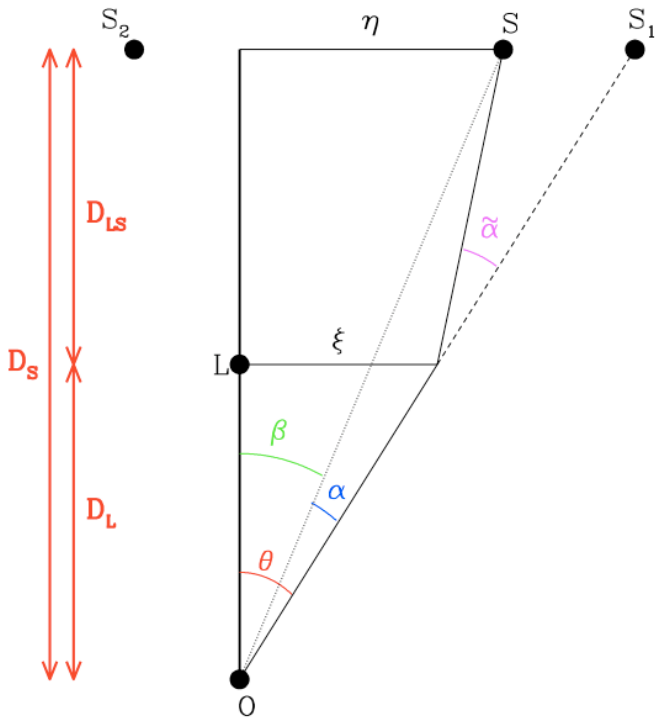

Gravitational Lensing; Basics

Several commonly used quantities in lensing are the **critical surface-mass density**, Σ_{crit} , and the the **Einstein Radius, R_E**.

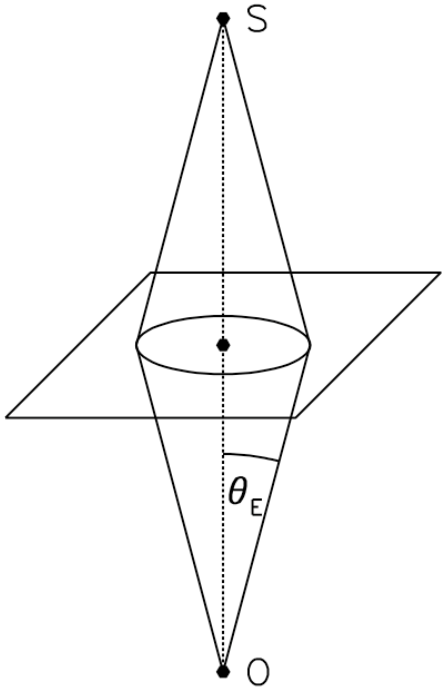

Multiple images are produced when the surface mass density of the lens exceeds the critical value :

$$\Sigma_{crit} = \frac{c^2}{4\pi G}\frac{D_s}{D_d D_{ds}}$$

$\Sigma_{crit} \sim 0.8$ g cm^{-2} for lens and source redshifts of 0.5 and 2.0, respectively.

For the special case in which the source lies exactly behind the lens ($\beta = 0$) a ring-like image is produced with a radius (commonly referred to as the **Einstein Radius**) θ_E :

$$\theta_E = \sqrt{\frac{4GM}{c^2}\frac{D_{ds}}{D_d D_{os}}} = (0.9)\left(\frac{M}{10^{11} M_{sun}}\right)^{1/2}\left(\frac{D_d D_{ds}/D_s}{Gpc}\right)^{1/2}$$

Gravitational Lensing; Basics

The magnification due to lensing of a point source obtains an infinite value at certain locations.
These locations are called **critical curves** in the lens plane (upper panel) and **caustics** in the source plane (lower panel). The numbers in the bottom panel identify regions in the source plane that correspond to 1,3 or 5 images, respectively.
Figure from J. Wambsganns, Gravitational Lensing in Astronomy, www.livingreviews.org/Articles/Volume1/1998-12wamb

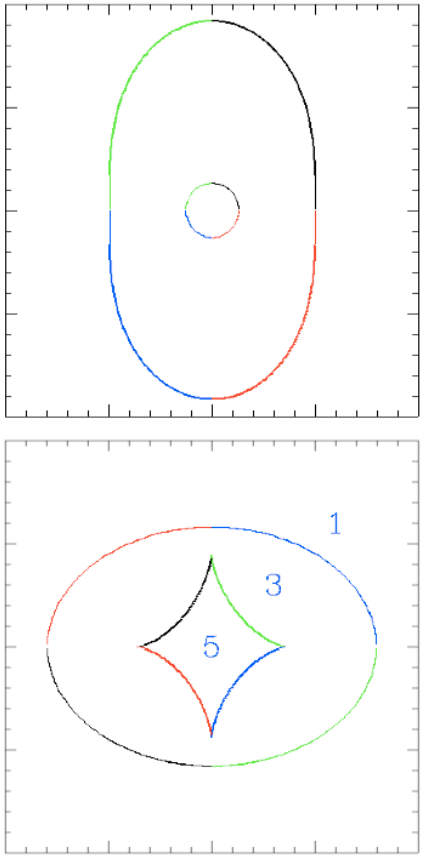

Gravitational Lensing; Basics

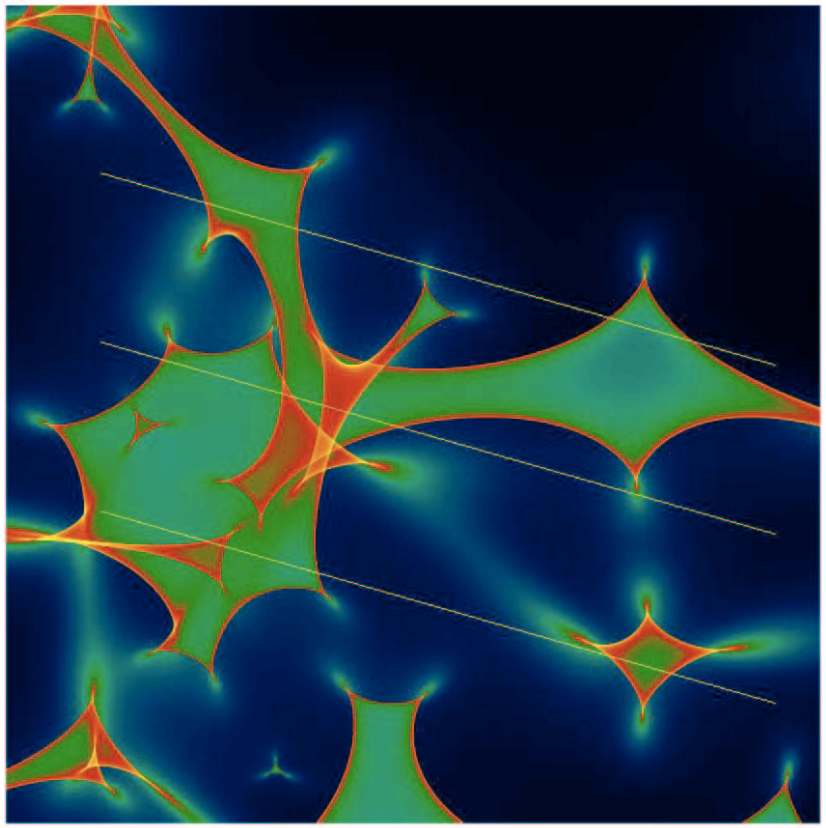

Figure 10: *Magnification pattern in the source plane, produced by a dense field of stars in the lensing galaxy. The color reflects the magnification as a function of the quasar position: the sequence blue-green-red-yellow indicates increasing magnification. Lightcurves taken along the yellow tracks are shown in Figure 11. The microlensing parameters were chosen according to a model for image A of the quadruple quasar Q2237+0305:* $\kappa = 0.36$, $\gamma = 0.44$.

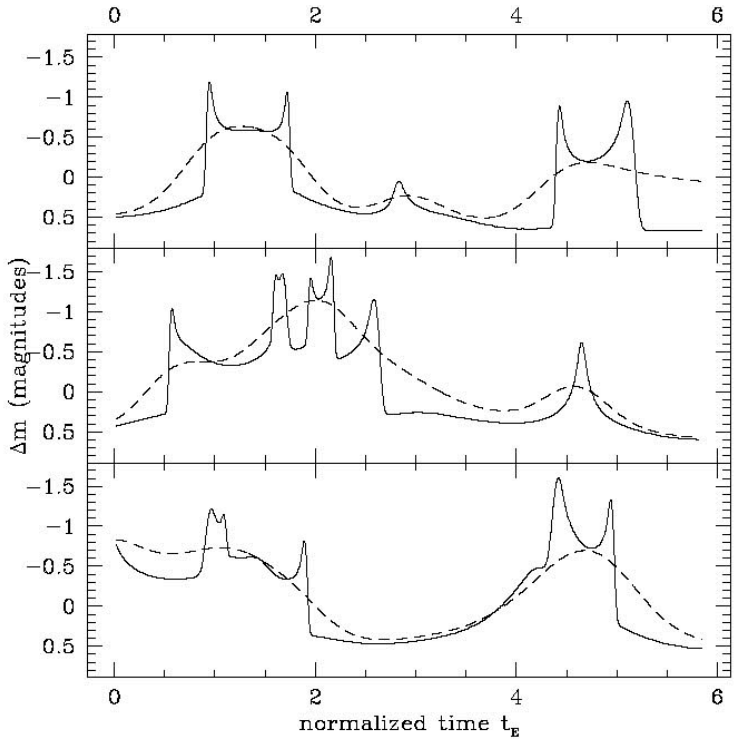

Figure 11: *Microlensing Lightcurve for the yellow tracks in Figure 10. The solid and dashed lines indicate relatively small and large quasar sizes. The time axis is in units of Einstein radii divided by unit velocity.*

Figures from J. Wambsganns, Gravitational Lensing in Astronomy, www.livingreviews.org/Articles/Volume1/1998-12wamb

Magnified Views of Quasars

- The large magnification factors of gravitationally lensed systems allow us to investigate the properties of quasars with X-ray luminosities that are substantially lower than those of unlensed ones.

Magnification Factors for Several GL Quasars

Object	z	M
HE 1104-1805	2.32	9.6-9.75[a]
B 1422+231	3.62	10[b]
PG 1115+080	1.72	19-24[c]
MG 0414+0534	2.64	28[b]
RXJ0911+0551	2.8	17[b]
APM08279+5255	3.91	50-100[d]

[A] 1104 From Wisotzki et al. 1998, 339, L73
[b] Dai et al. 2003, in preparation
[c] From Impey et al. 1998, ApJ, 509, 551, the range in magnification values reflects the range of lens models used to fit the data.
[d] Egami et al. 2000

Magnified Views of Quasar Outflows

3rd INTERNATIONAL X-RAY ASTRONOMY SCHOOL

Magnified Views of Quasar Outflows

- Present X-ray data for Broad Absorption Line QSOs (BALQSOs) are sparse and only poor to moderate S/N spectra are available.

- X-ray faintness is likely due to absorption with N_H ranging from 10^{22} to 10^{24} cm^{-2} (Kopko, Turnshek, & Espey 1994; Green & Mathur 1996; Gallagher et al. 1999; Mathur et al. 2000)

- Their power-law continua are typical of normal quasars, with $\Gamma \sim 2$, and a_{ox} ranging from -1.70 to -1.44

- The flux magnification of the two BALQSOs APM08279+5255 and PG1115+080, estimated to be ~100 and ~25 in the X-ray band, and their high redshift of $z = 3.91$ and $z = 1.72$ respectively, have allowed the study of the kinematic and ionization properties of BALQSOs in the X-ray band.

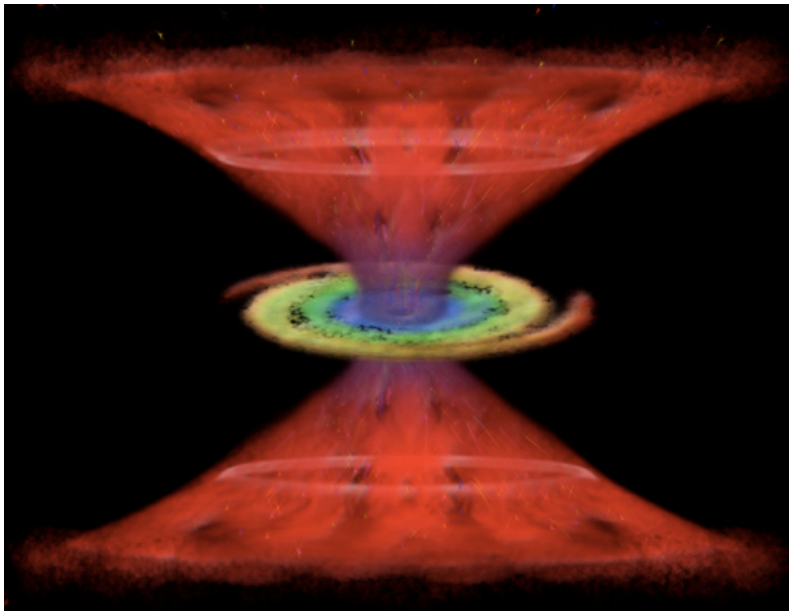

It is commonly accepted within the AGN community that most quasars contain high velocity winds of highly ionized gas flowing away from the central source at speeds ranging between 5,000 and 30,000 km s^{-1}

The Importance of Quasar Outflows:

- Quasar outflows may distribute a significant amount of accretion-disk material into the interstellar and intergalactic medium.

- Quasar outflows may be important in regulating the coeval growth of black holes and their host galaxies (e.g., Fabian 1999)

- Quasar winds possibly provide a mechanism for angular momentum loss from the accretion disk

- It has been proposed that quasar outflows may be a source for cosmic dust

(e.g., Elvis, 2002)

Unanswered Questions Regarding Quasar Outflows :

(a) Is the X-ray absorption in BALQSOs due to the out-flowing wind? If so what are the kinematic properties of the X-ray absorbing medium?

(b) What are the ionization properties of the X-ray absorbers (N_H, n, U) and are they consistent with ionization properties of the UV absorber?

(c) Is the X-ray absorber the postulated shielding gas?

(d) Is the X-ray continuum from the primary source observed directly?

(e) Why is there a lack of variability in the velocity structures of UV BALs? (e.g., Barlow 1993; Proga et al. 1995) Is this true for X-ray BALs?

(f) Are low ionization BALQSOs quasars at an early stage in their evolution?

Magnified Views of BALQSO APM 08279+5255

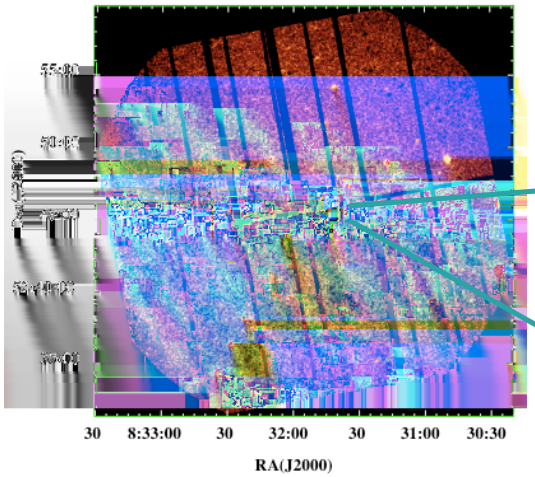

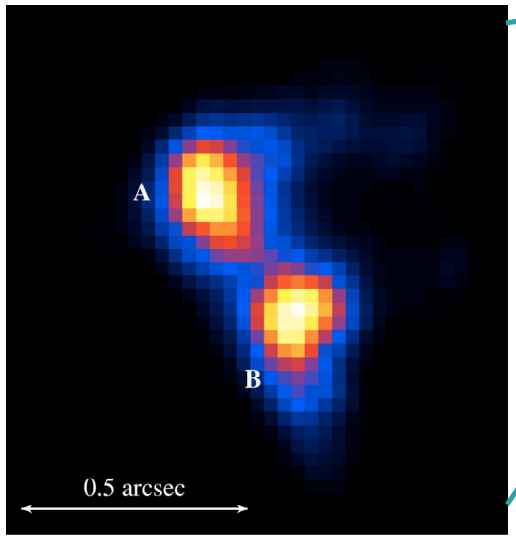

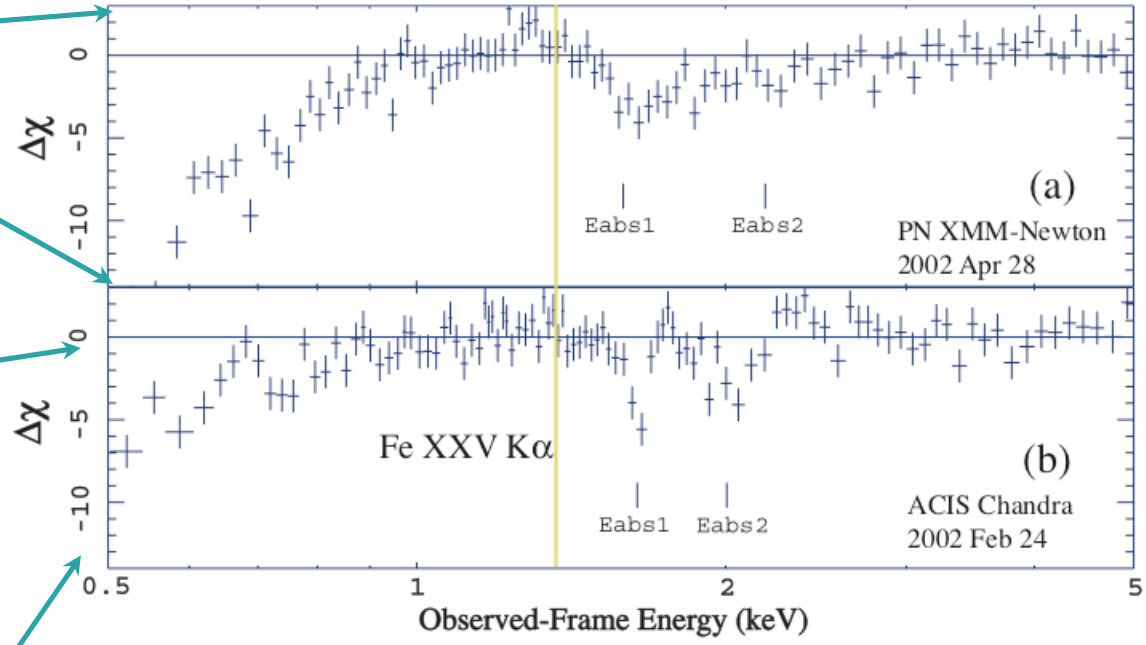

Blueshifted Fe XXV Ka absorption lines (a) *XMM-Newton* Spectrum (b) *Chandra* Spectrum of APM08279+5255. We find significant variability of the X-ray BALs on rest-frame timescale of 1.8 weeks.

Magnified Views of BALQSO PG 1115+080

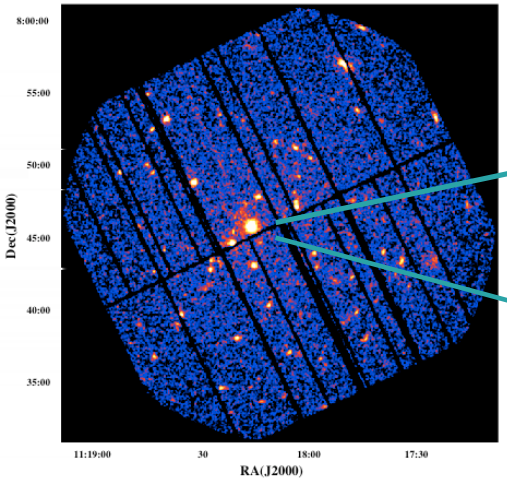

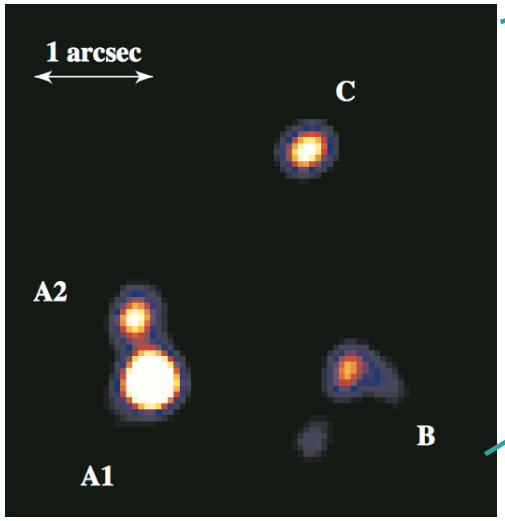

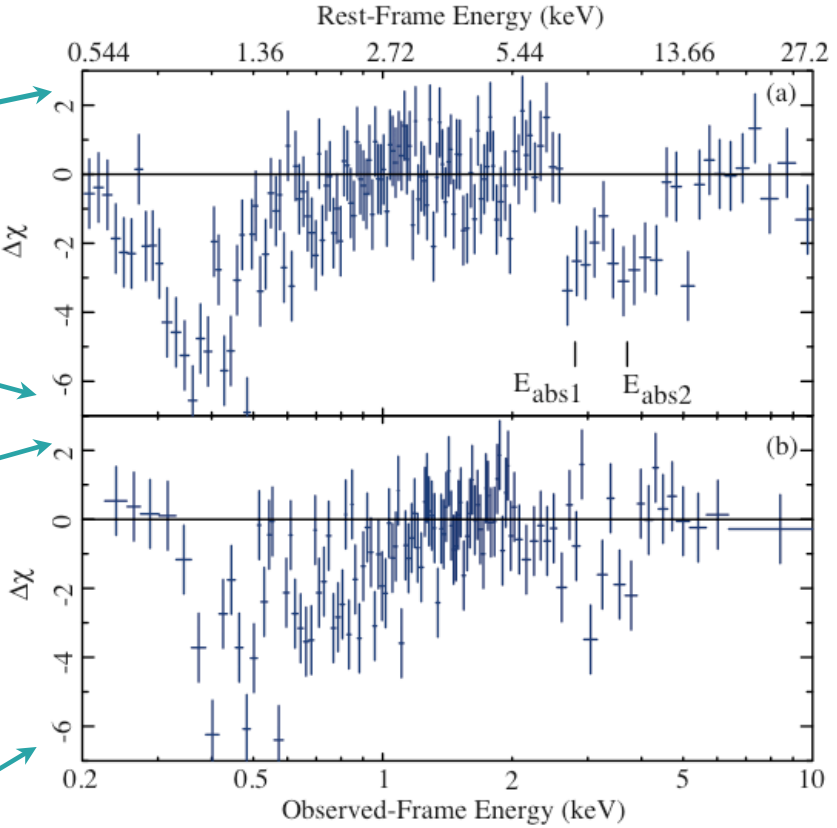

Blueshifted Fe XXV Ka absorption lines (a) XMM-Newton Spectrum (b) Chandra Spectrum of PG 1115+080. We place a weak constraint on variability of the X-ray BALs on rest-frame timescale of 19 weeks.

Magnified Views of BALQSOs

Discussion of Spectral Results

- A plausible site that may be producing the absorption features is the quasar wind. We propose that the observed high-energy absorption lines are associated with Fe K resonant absorption.

- The rest energies of the most likely resonant absorption lines of Fe are:

  6.70 keV (Fe XXV Ka), 7.88 keV (Fe XXV Kb), 6.97 keV (Fe XXVI Ka), 8.25 keV (Fe XXVI Kb)

  (Verner, D. A., Verner E. M., & Ferland, G. J., 1996, Atomic Nucl. Data)

- **APM 08279+5255** : The 8.05+/-0.1 keV and 9.79+/-0.2 keV absorption features correspond to wind velocities of 0.20*c* (Fe XXV Ka), 0.15*c* (Fe XXVI Ka), and 0.40*c* (Fe XXV Ka), 0.36*c* (Fe XXVI Ka), respectively.

- **PG1115+080** : The rest-frame energies of 7.38 keV and 9.5 keV imply outflow velocities of about 0.1*c* (Fe XXV Ka), 0.04*c* (Fe XXVI Ka), and 0.34*c* (Fe XXV Ka), 0.30*c* (Fe XXVI Ka), respectively.

Magnified Views of BALQSOs

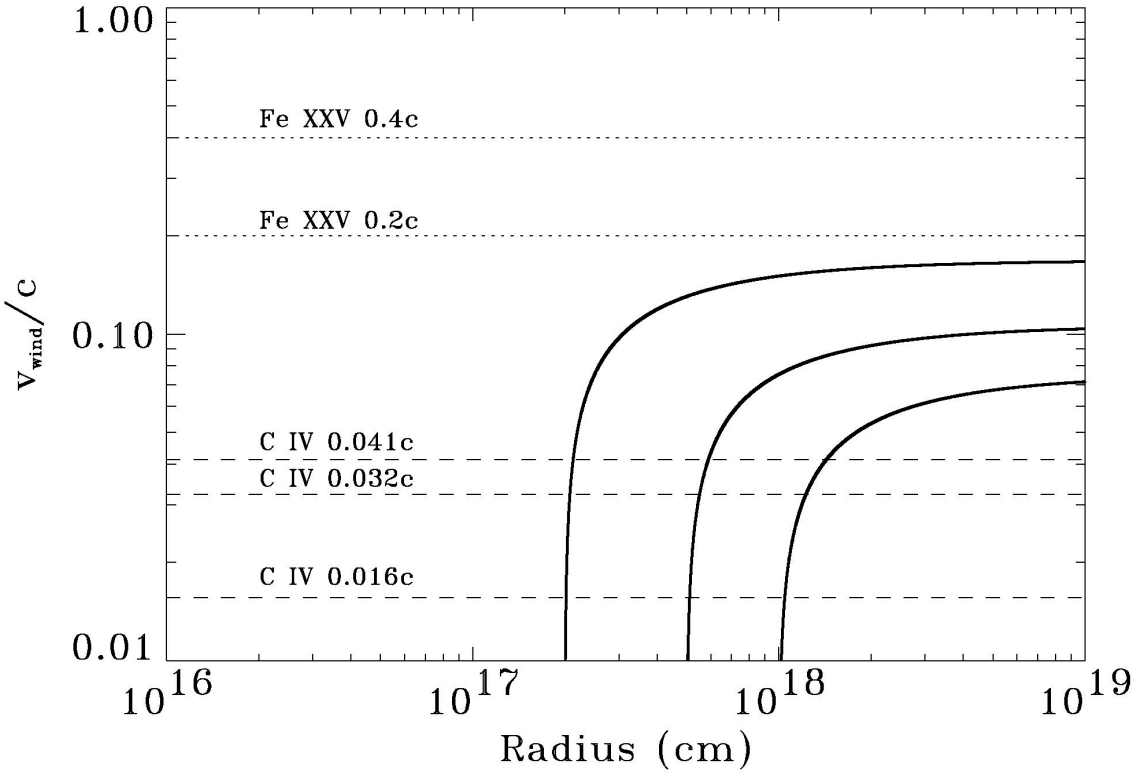

Wind velocity as a function of radius from the central source for a radiation pressure driven wind.
For a qualitative comparison we have estimated the wind velocities for launching radii of 2 x 10^{17} cm,
5 x 10^{17} cm, and 1 x 10^{18} cm. We have over-plotted the observed C iv BAL (dashed lines) and Fe xxv BAL (dotted lines) velocities. We have assumed G_f=100, L_{UV}=4x10^{46} erg/s, L_{Bol} = 2x10^{47} erg/s and L_{Bol}/L_{Edd} = 0.1.

Imaging of AGN Accretion Disks via Microlensing

3rd INTERNATIONAL X-RAY ASTRONOMY SCHOOL

Imaging of AGN Accretion Disks via Microlensing

- Direct imaging of accretion disks requires angular resolutions of the order of tens of nano-seconds at z ~1.
- Indirect Mapping Methods

Reverberation Mapping of BLR (Blandford & McKee 1982, Peterson 1993, Netzer & Peterson 1997) This method relies on the time lag between variations in the flux from a central source of ionizing radiation and the response of the emission lines from photoionized gas in the broad line region. (successfuly used to determine the size of the broad line region in several AGN) *driver:* central source of ionizing radiation, *receiver:* photoionized gas in the broad line region

Reverberation Mapping of the Fe Ka Emission Region (Young & Reynolds 2000) This method relies on the variation of the profiles of the Fe Ka fluorescence lines originating in the inner parts of the disk. *driver:* X-ray continuum source near BH, *receiver:* cold gas in accretion disk

Microlensing of Accretion Disk Continuum Emission (Grieger et al. 1988 and 1991; Schneider, Ehlers & Falco 1992; Gould & Gaudi 1997; Agol & Krolik 1999; Yonehara et al. 1999; Mineshige & Yonehara 1999) This method exploits the high magnification microlensing events (HMEs) in lensed quasars. During a microlensing event magnification caustics produced by stars in the lensing galaxy traverse the plane of the accretion disk and selectively magnify different emission regions. An analysis of the light-curves of microlensing events obtained in several wavelengths can be used to infer the surface brightness and inclination angle of the accretion disk. First detection of microlensing event in the Einstein Cross (Irwin et al. 1989). Limits on source size (Wambsganss et al., 1990; Wyithe, Webster , & Turner 1999 and 2000; Yonehara, 2001, Shalyapin 2001)

Microlensing of the Fe Ka Emission Region (Chartas et al. 2002, Popovic et al. 2003)

Imaging of AGN Accretion Disks via Microlensing

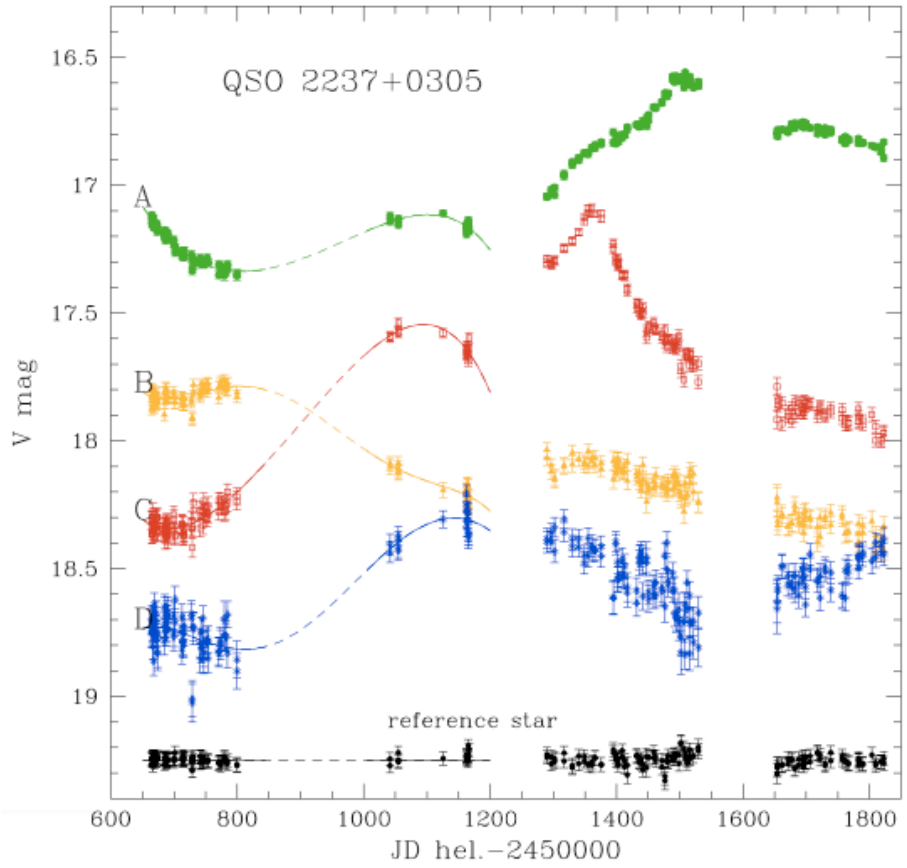

Light curves of the lensed images of QSO 2237+0305. Also shown is the light curve of the 18.14 mag reference star shifted by 1.1mag for clarity (figure obtained from the The Optical Gravitational Lensing Experiment (OGLE) monitoring of QSO 2237+0305; Udalski et al. 1999}

Imaging of AGN Accretion Disks via Microlensing

Microlensing of the Fe Ka emission Region

A useful scale in microlensing is the **Einstein Radius** :

$$\eta_E = [(4GM_{star}/c^2)(D_{OS}D_{LS}/D_{OL})]^{1/2}$$

Where, M_{star} is the mass of the star in the lens plane and D represents the angular diameter distances.

For MG J0414+0534, z_{lens}=0.96 and z_{source} =2.64 we have:

$$\eta_E \sim 0.01(M_{star}/M_{solar})^{1/2} \text{ pc}$$

Crossing time scale : $t_E = \eta_E/v_t$ and $t_{HME} \sim c_{HME}r_s/v_t$

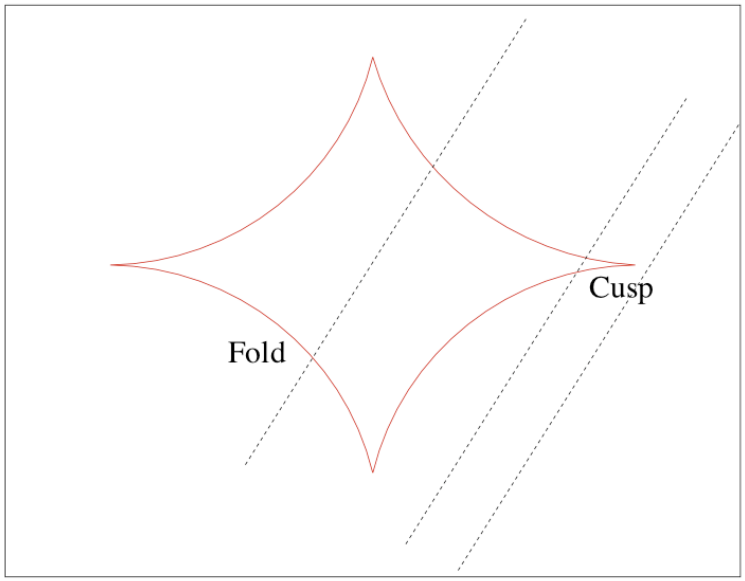

Caustic of a single star plus shear. Three tracks are shown of sources crossing fold and cusp caustics.

Imaging of AGN Accretion Disks via Microlensing

3rd INTERNATIONAL X-RAY ASTRONOMY SCHOOL

Imaging of AGN Accretion Disks via Microlensing

Microlensing of the Fe Ka emission Region

The amplification of a point source by a fold caustic is::

$$A = A_0 + K(x - x_c)^{-1/2} H(x - xc)$$

where $K \sim (\square_E/r_g)^{1/2}$ and $r_g = GM/c^2$

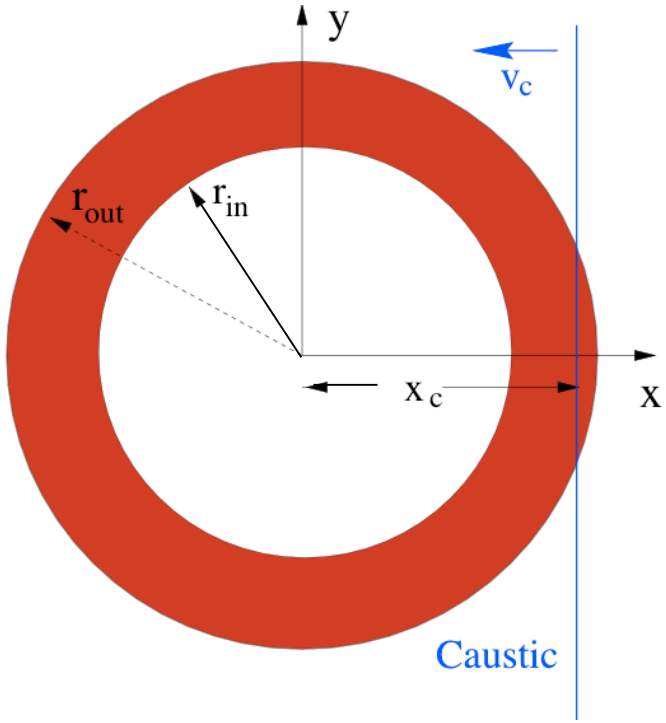

Schematic of a caustic traversing an accretion disk. The line parallel to the y axis is the fold caustic. The disk axis points out of the page.

Imaging of AGN Accretion Disks via Microlensing

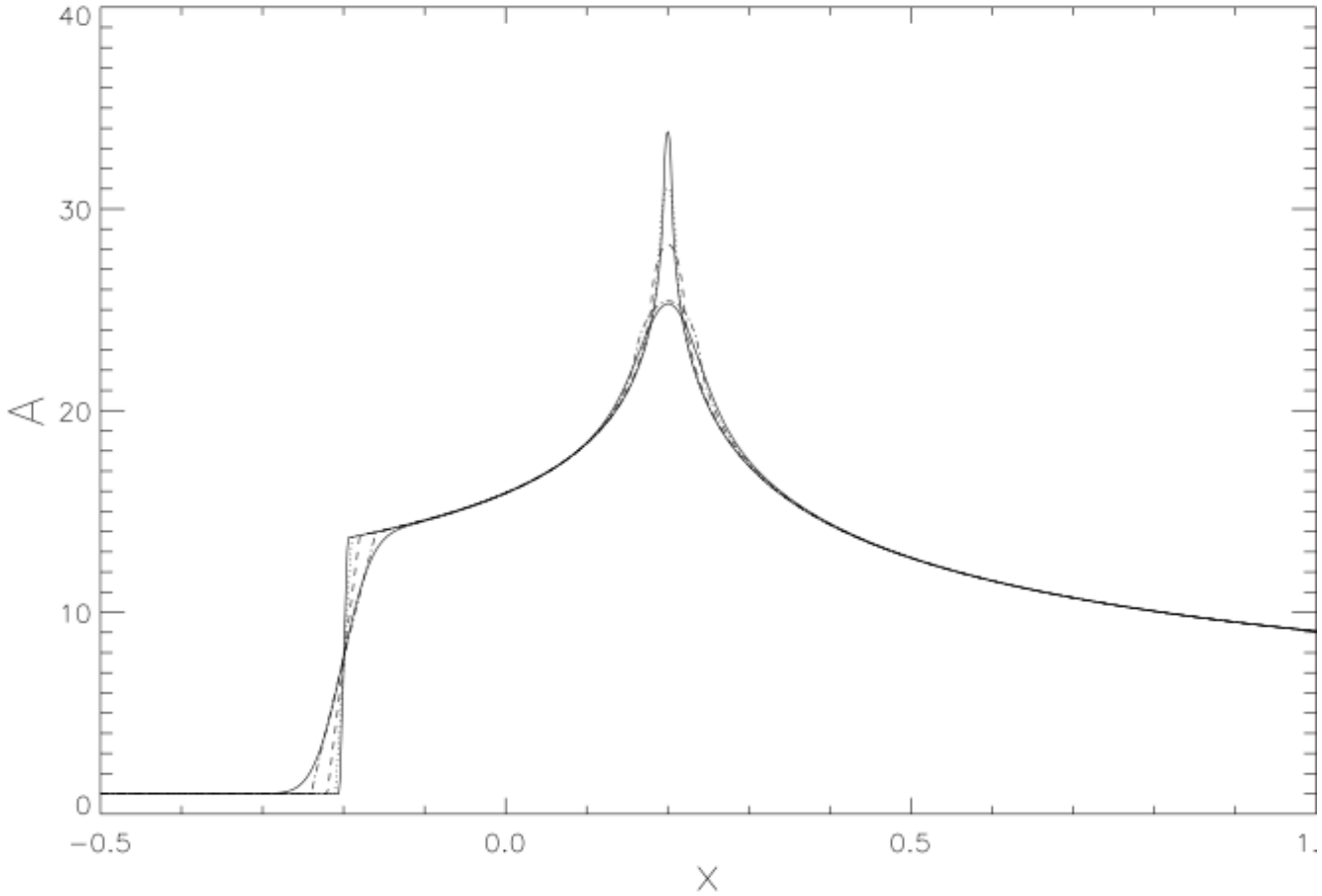

The amplification of a ring-shaped emission region by a straight fold caustic as a function of the distance of the caustic from the center of the ring.

Imaging of AGN Accretion Disks via Microlensing

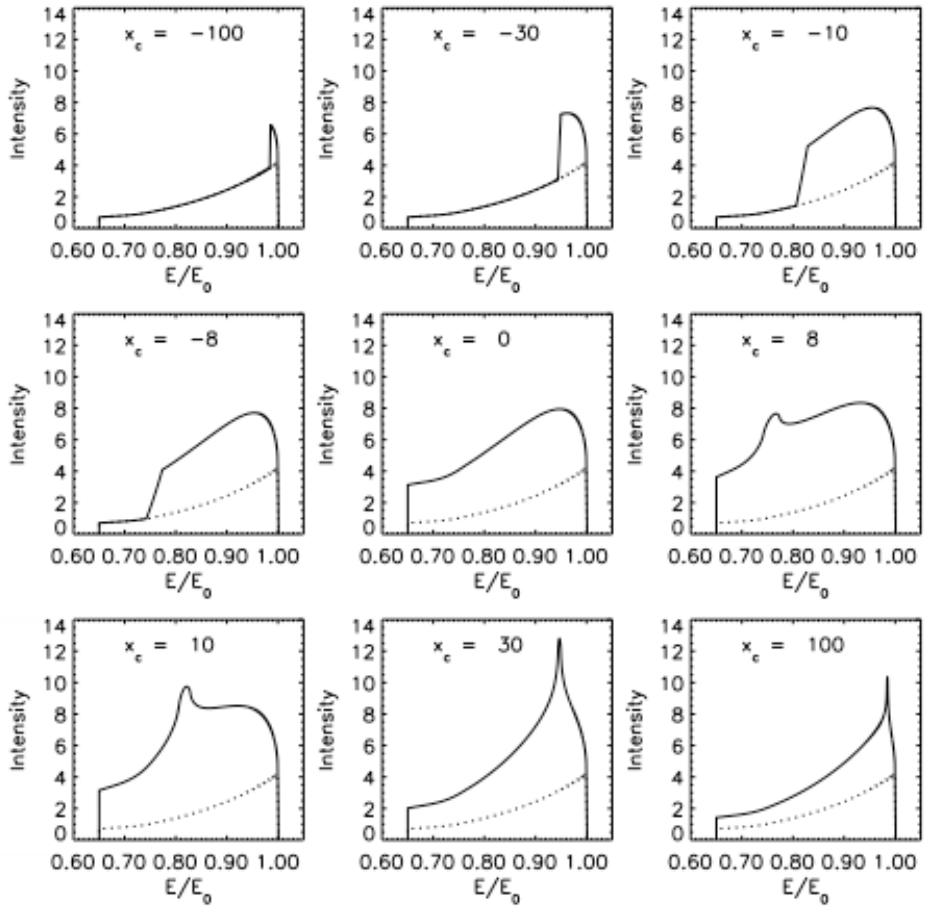

Simulations of the evolution of the Fe K line profile as the caustic traverses a face-on accretion disk around a Schwarzchild black hole. x_c is the distance of the caustic from the center of the accretion disk in units of gravitational radii. The caustic strength used for the simulations is $K/A_0 = 10 r_g^{1/2}$. The assumed velocity broadening of the iron line in the rest frame of the disk is $\sigma_v/v = 0.01$, where v is the Keplerian rotation velocity.

Imaging of AGN Accretion Disks via Fe Ka Microlensing

- A candidate quasar for imaging the accretion disk via Fe Ka microlensing is MG 0414+0534.
- MG J0414+0534 was discovered by Hewitt et al., 1992. $z_{lens} = 0.96$ (Tonry & Kochanek, 1999), $z_{source} = 2.64$ (Lawrence, 1995)
- Components of this system are exceedingly red with R-H colors of 6.8 mag for image C, 3.2 mag for the arc and 3.2 mag for the lens galaxy.
- Time delays : $\Delta t_{A1B} = 15.7$ +/- 1.3 days, $\Delta t_{A2B} = 16$ +/- 1.4 days, $\Delta t_{CB} = 66$ +/- 5 days
- Magnifications : $M_{A1} \sim 12.4$, $M_{A2} \sim 14.1$, $M_B \sim 5.1$, $M_C \sim 1.8$

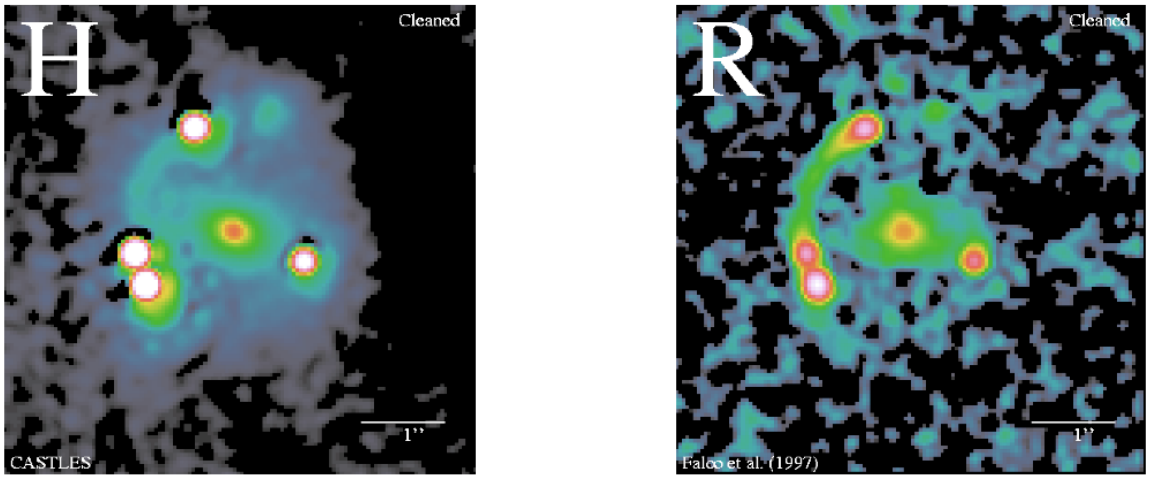

(left panel) HST H band and (right panel) HST R band image of MG~J0414+0534

Imaging of AGN Accretion Disks via Fe Ka Microlensing

Chandra Monitoring of MG 0414+0534

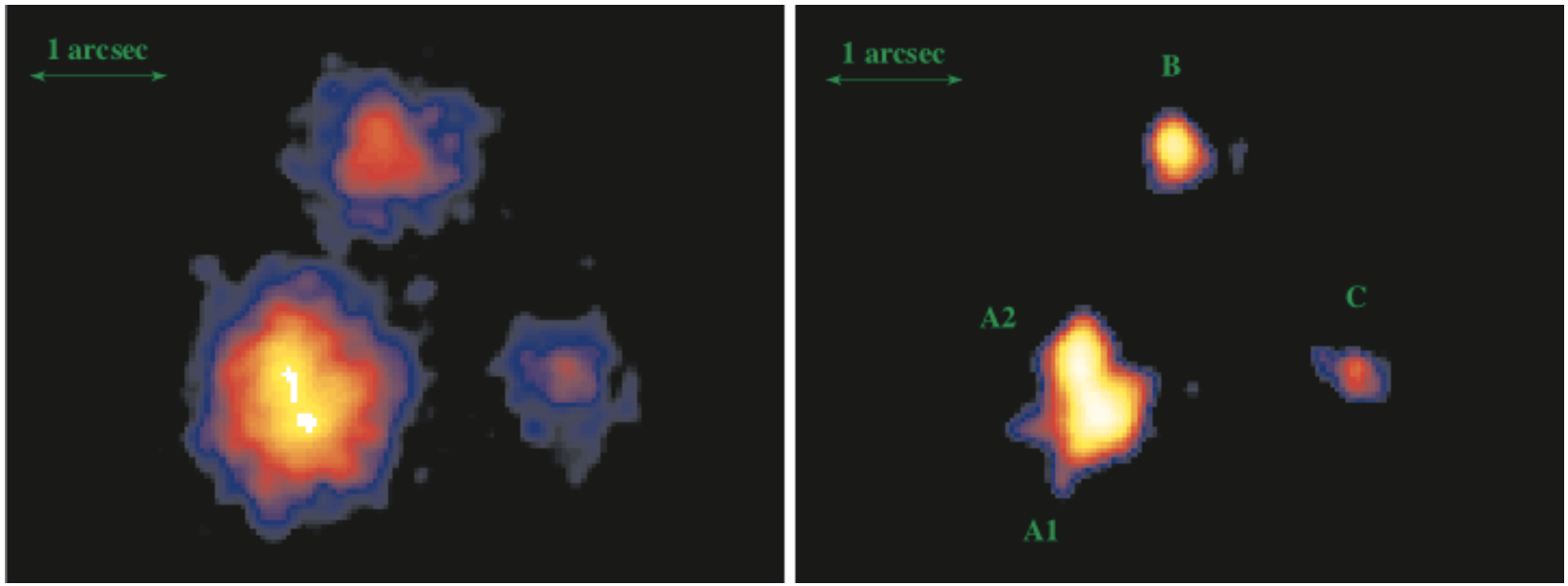

(left panel) Combined image of five Chandra observations of MG 0414+0534, (rigth panel) Deconvolved image

Imaging of AGN Accretion Disks via Fe Ka Microlensing

The interval between the first detection of the Fe-K line (EW ~ 900eV) in image B (panel b) and the second DDT observation (panel d) is about 1.2 years (observed frame). The timescale of this particular microlensing event is :

$$t_e \sim 2(R_s/10^{15}\,\mathrm{cm})\ \mathrm{years}$$

where R_s is the size of the continuum emission region. The continuum region must be $R_s < 0.6\mathrm{x}10^{15}\mathrm{cm}$.

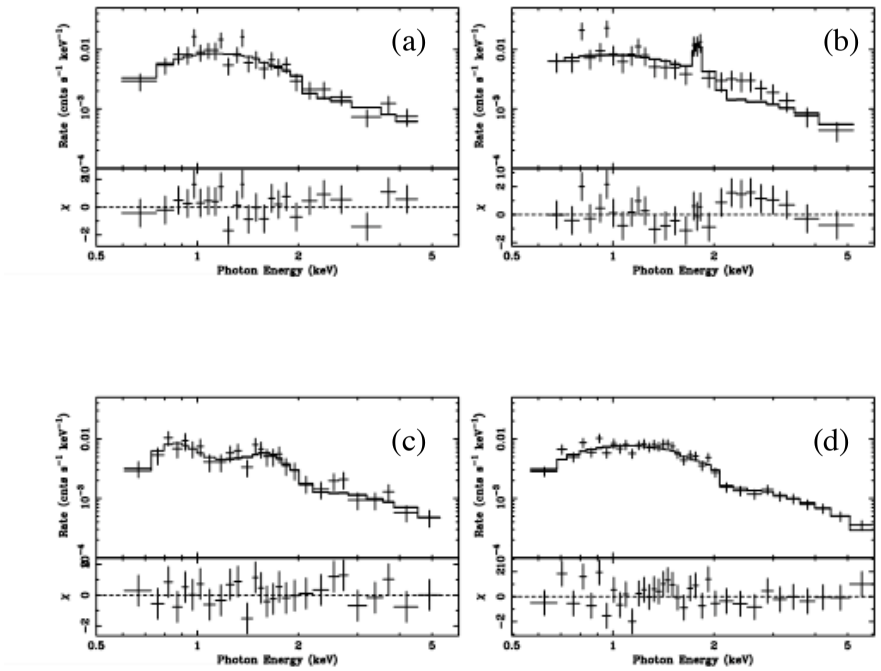

Evolution of the spectrum of image B of MG J0414+0534 over 2.2 years.

Constraining Cosmological Parameters

3rd INTERNATIONAL X-RAY ASTRONOMY SCHOOL

Deriving H_0 using Gravitational Lenses

The time delay between image i and an unlensed light path is:

$$\tau_i = \frac{(1+z_d)}{2c} D|\theta_i - \beta|^2 - \frac{(1+z_d)}{c^3}\psi(\theta_i)$$

Geometric Time Delay — Shapiro Time Delay

The dependence of $\Delta\tau_{ij}$ (time delay) on the Hubble parameter H_0 is embedded in $D = D_d D_s / D_{ds} \propto H_0^{-1}$.

$$\frac{c\Delta\tau_{ij}}{(1+z_d)D} = Function[Observables + Lens\ Model]$$

Constraining Cosmological Parameters

- With a good lens model, image positions, time delays and kinematic constraints of the lens we can estimate H_0

- Alternatively, one may use an indepentently measured value of H_0 (e.g., WMAP, HSTKP) to constrain the dark mater distribution of the lensing galaxy.

- The main difficulty in measuring time-delays is that the brightness of each image has to be carefully monitored over several periods of the time-delay and the quasar has to show sufficient variability over time scales smaller than the time-delay.

- X-ray observations of several GL quasars, show strong variability over time scales of hours to days.

Constraining Cosmological Parameters

The detection of a rapid flare in a *Chandra* observation of RX J0911.4+0551 indicated that it was possible to measure "short" time-delays in GL systems with accuracies of a few percent and within a single observation.

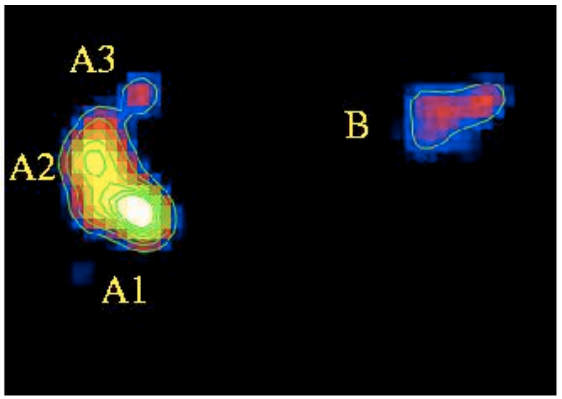

- RXJ0911 was first detected from the ROSAT ALL-Sky Survey (Bade et al. 1995)
- RXJ0911 is a quadruply lensed quasar at z=2.8, with the lens a galaxy + cluster at $z = 0.77$
- Observed with *Chandra* on Nov 2 1999 for 29 ks
- Proposed method to measure short time-delays (Chartas et al. 2001)
- Estimated $\Delta t_{AB} = 0.65 h^{-1}$ days

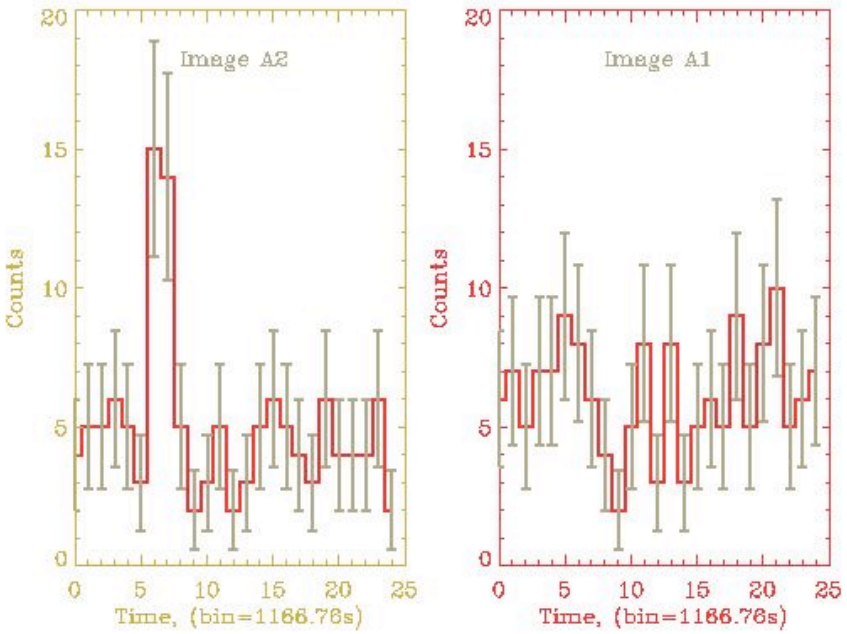

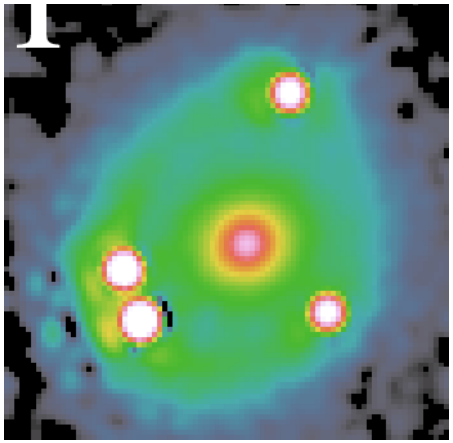

HST H band (Castles)

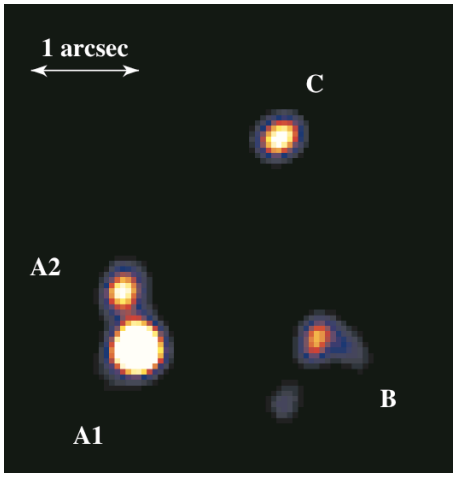

Deconvolution of *Chandra* 10ks image of PG1115

Measurements of short time delays in PG 1115+080

- PG1115+080 $z_s = 1.722$, $z_l = 0.311$
- The source is a mini broad absorption line quasar with a OVI wind velocity of 6,000km/s
- Observed with *Chandra* on June 2 and Nov 3 2000 for 26.8ks and 10ks respectively, and was observed with *XMM-Newton* on Nov 25 2001 for 62.6ks.

Flux Ratios

Band	A1	A2	B	C
X-ray	3.73+/-0.12	0.85+/-0.07	1.08+/-0.06	1
HST H	4.06+/-0.17	2.56+/-0.12	0.65+/-0.04	1

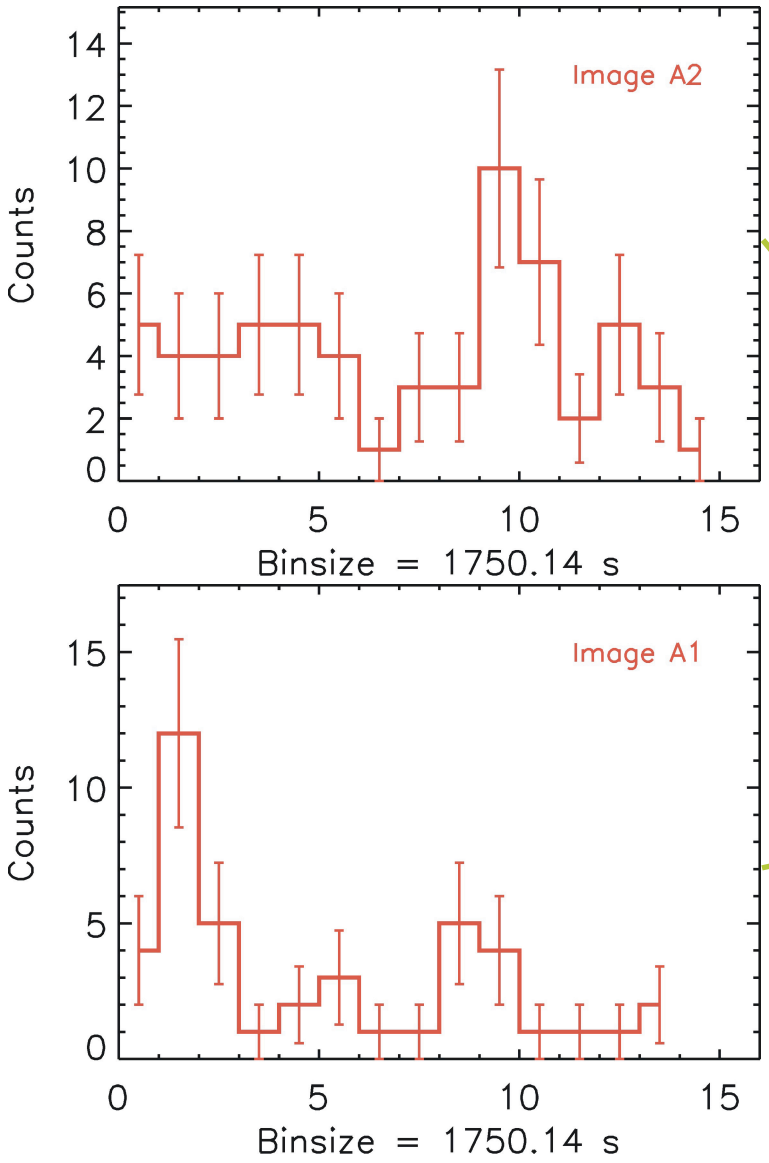

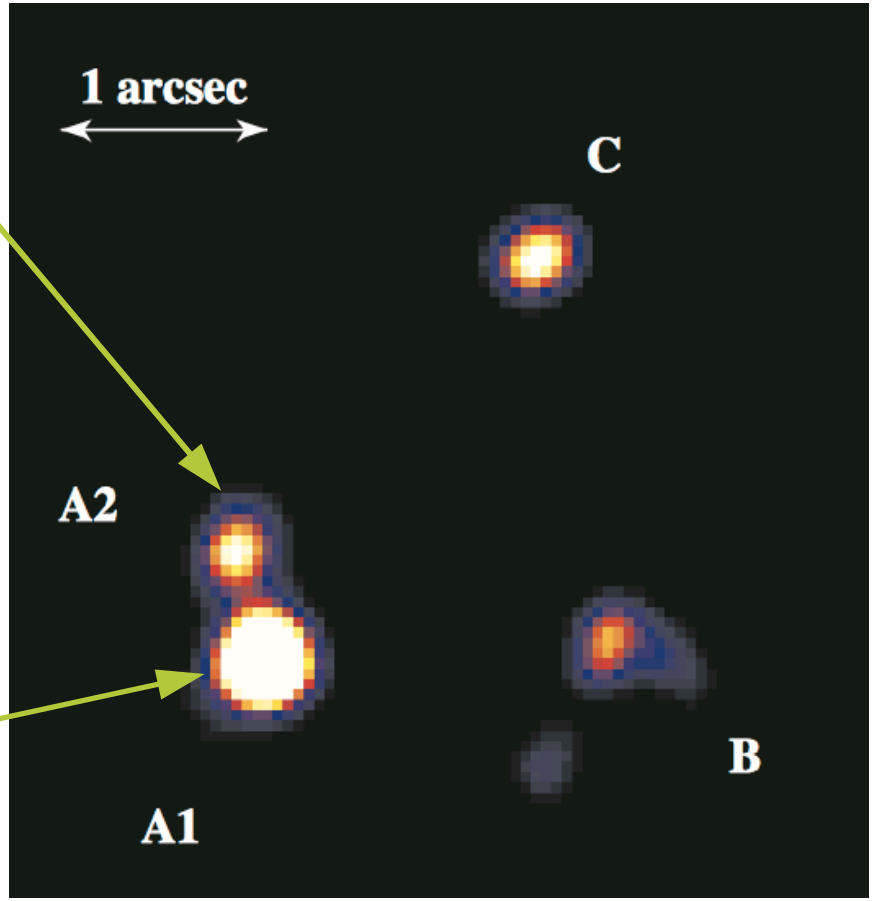

Δt_{A1A2} = 0.16 (-0.02,+0.02) days

Constraining Cosmological Parameters

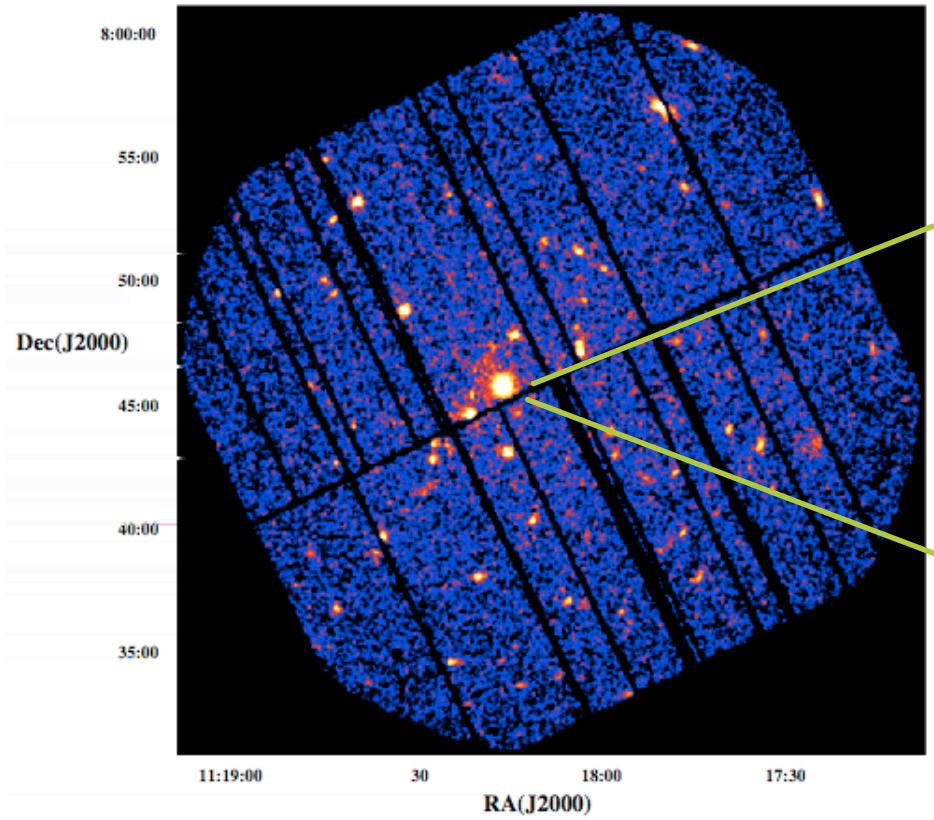

XMM-Newton image of PG1115+080 field

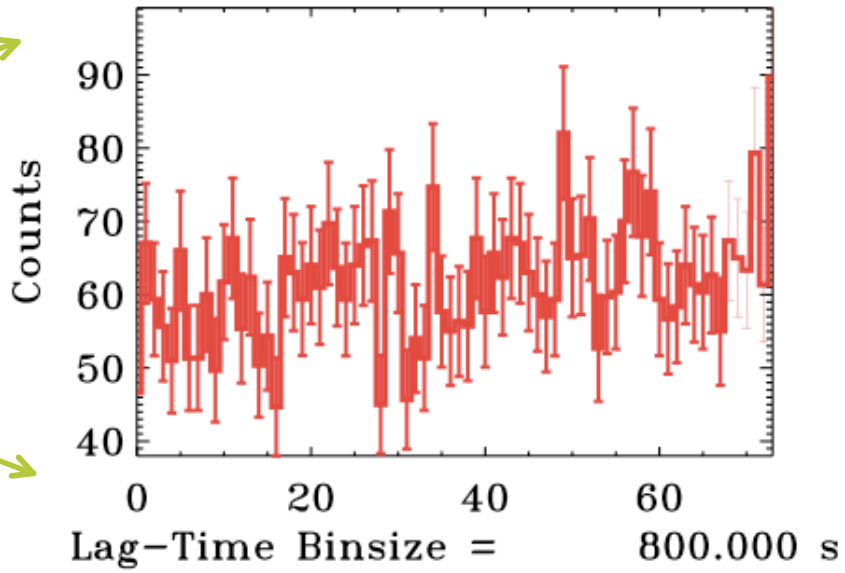

Light Curve of PG 1115+080 in the 0.6 - 1.7 keV band taken with the PN instrument onboard *XMM-Newton*

Constraining Cosmological Parameters

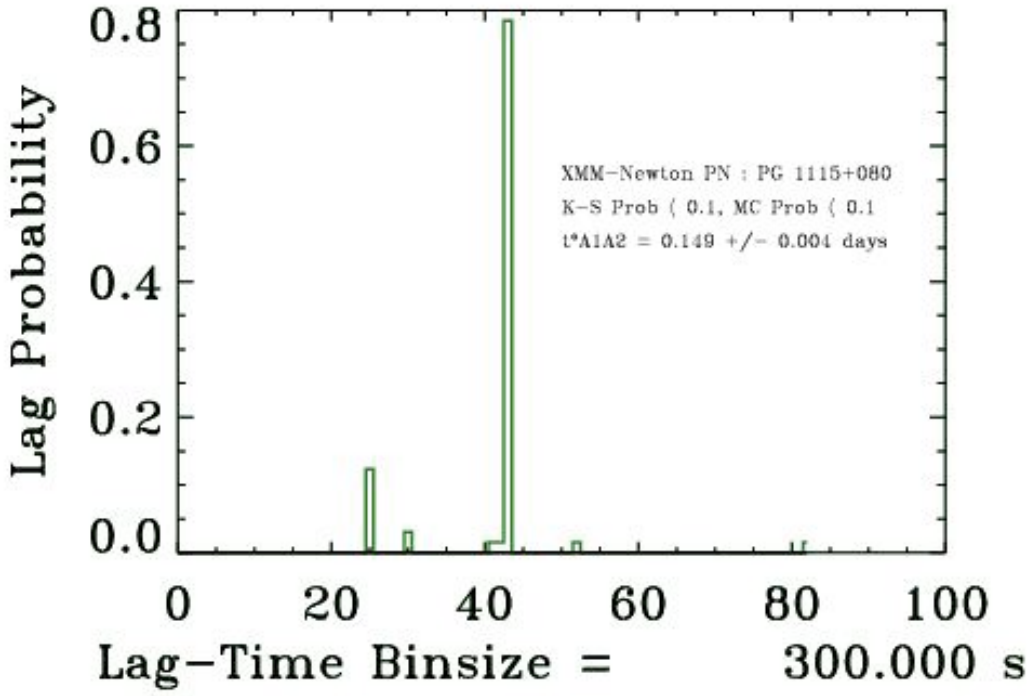

Δt_{A1A2} = 0.149 +/- 0.004 days

Auto-correlations (ACs) are performed to the combined *XMM-Newton* light-curves of all images of PG1115+080 over a range of energy bands. We plot the histogram of the AC lag times corresponding to the maxima of the AC coefficients with K-S chance probabilities of variability in each light-curve of less than 0.1 and Monte-Carlo chance probabilities of obtaining each AC coefficient of less than 0.1.

Constraining Cosmological Parameters

- The values for H_0 derived from present measurement of "long" time delays depend strongly on the assumed mass profiles of the lenses (e.g., Impey et al. 1998, Kochanek 2002).

Isothermal lens models predict $H_0 \sim 40\text{-}50 \text{km s}^{-1} \text{Mpc}^{-1}$,
Constant M/L ratio models predict $H_0 \sim 60\text{-}80 \text{km s}^{-1} \text{Mpc}^{-1}$

- The accurate X-ray measurement of the time delay $\Delta t_{A1A2} = 0.149 +/- 0.004$ in PG1115+080 was used to discriminate between mass models.

- Keeton's gravitational lensing software **gravlens** was used to produce a range of lens models (e.g., lens model by True & Koopmans 2002) , fit these models to the observables and predict the time-delays for each model. This method results in a value of :

$$H_0 = 67\ (-8,+13) \text{ km s}^{-1} \text{Mpc}^{-1}$$

consistent with WMAP and HSTKP results.

Future Prospects

Constrain the Mass Outflow rate of Quasars

Observations of gravitationally lensed BALQSOs with the next generation high-throughput X-ray telescopes (e.g., Constellation-X) will allow us to constrain the absorbing, ionization and kinematic properties of the X-ray BAL material and thus provide tighter constraint on the mass outflow rate of the wind. These observations will ultimatelly allow us to estimate the contribution of quasar outflows to the enrichment of the ISM and IGM.

Image an AGN Accretion Disk via Fe Ka Microlensing

The next generation high-throughput X-ray telescopes will allow us to directly probe the various emission regions of an accretion disk from scales of a few hundred gravitational radii down to the event horizon of the black hole. We expect to achieve this goal by monitoring changes in the line energy, intensity, and profile of the Fe~Ka line in gravitational lensed systems that are undergoing microlensing events.

Map Accretion Disk Flares in Quasars

Recently **Yonehara et al. 2003** proposed a method to map the locations of accretion disk flares in quasars.

The technique will require observations of gravitationally lensed quasars in the X-ray band with telescopes having subarcsec resolution and collecting areas of the order of 10000 cm^2.

The method is based on the following equation that provides a relation between the location of flares and the difference in time delays produced by these flares.:

$$\Delta\tau = \frac{(1+z_l)}{c}\frac{D_{ol}}{D_{ls}}\left[\left(\vec{\theta}_i - \vec{\theta}_j\right)\cdot\vec{r}\right]$$

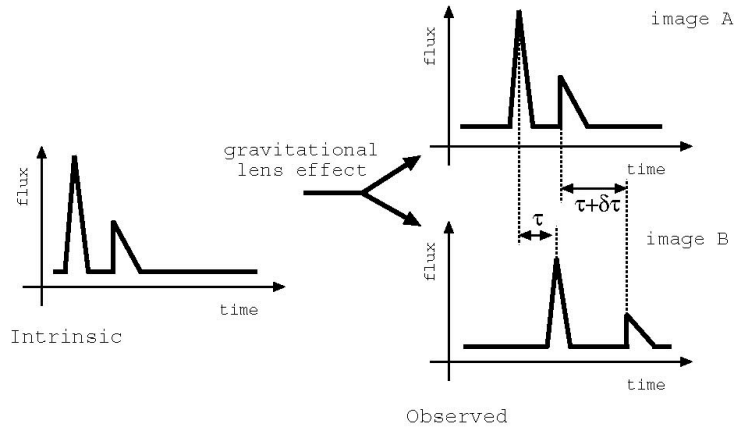

Fig. 2.— Schematic plots of the difference in the time delay between different flares in the same image pair of a lensed quasar.

Chincoteague 2003









3rd INTERNATIONAL X-RAY ASTRONOMY SCHOOL